Reports

Discovery of a New Gravitational Lens System

Abstract. *A new gravitational lens system, the triple radio source MG2016+112, has been discovered. Five emission lines at a redshift of 3.2733 ± 0.0014 have been identified in the spectra of two stellar objects of magnitude 22.5 coincident with radio components 3.4 arc seconds apart. The lines are the narrowest ever observed in objects at such a large redshift. The redshift of a 23rd-magnitude extended optical object coincident with the third radio component has not been determined spectroscopically, but its known optical properties are consistent with those of a giant elliptical galaxy with a redshift of about 0.8.*

The formation of multiple images of a distant object by the gravitational effects of an intervening object was mentioned by Eddington (*1*) in 1920 and by Zwicky (*2*) in 1937. Details of image formation were calculated by Einstein (*3*) in 1936, and subsequently discussed by many others. The first example of lensing, the radio source 0957+561, was found in 1979 (*4*), and two optical examples have been discovered since then (*5*). We report the discovery of a new system, the radio source 2016+112, and describe a procedure for finding many more examples.

Imaging by gravitational lenses depends on the mass distribution of the lensing object. Cosmological effects are important, since the lensed objects are in general extremely distant. Gravitational lensing thus provides a potentially powerful tool for investigating two of the outstanding problems in astronomy: the distribution of mass in galaxies and clusters of galaxies, and the values of three fundamental cosmological parameters, H_0, q_0, and Λ (*6*). Significant progress on these important problems through the use of gravitational lensing will require either a statistical sample of lenses, or a few particularly simple or special cases.

The radio source 2016+112 was first detected in the MIT–Green Bank (MG) 6-cm survey (*7*), made with the 300-foot transit telescope of the National Radio Astronomy Observatory (*8*). A high-resolution map obtained in May 1981 with the 27-antenna Very Large Array (VLA) of the National Radio Astronomy Observatory (NRAO) revealed three unresolved components. The source was reobserved at the VLA in February 1982 for 10 minutes at both 6 cm (4.885 GHz) and 20 cm (1.465 GHz), with synthesized beams (full width at half maximum) of 0.4 and 1.3 arc seconds, respectively. The 6-cm map is shown in Fig. 1, and the positions and fluxes of the three components are given in Table 1. Components A and B are separated by 3.4 arc seconds; C is 2.0 arc seconds from B. Many extragalactic radio sources are synchrotron sources, with a power law spectrum $S \propto \nu^{-\alpha}$, and α, the *spectral index*, is listed in the last column of Table 1 for the three components. The spectral indices of A and B are essentially the same, while C has a much flatter spectrum.

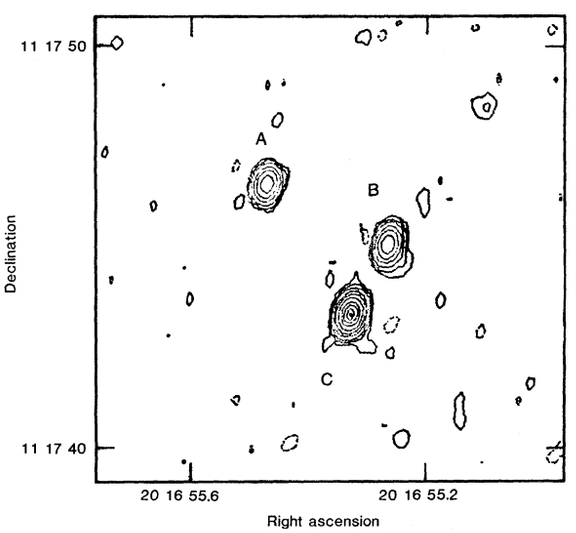

Fig. 1. VLA map of 2016+112 at 6 cm. Contour levels are −0.5 (dashed lines), 0.5, 1, 2, 5, 10, 20, 40, 60, 80, and 95 percent of 65 mJy, the peak level. The flux densities listed in Table 1 were obtained by Gaussian fits to the individual components. All three components are unresolved.

On the nights of 7 and 12 August 1983, direct images of the field were obtained in the 6000 to 7000 Å *r* photometric band (*9*), using the Prime Focus Universal Extragalactic Instrument (PFUEI) charge-coupled device (CCD) detector on the Palomar 200-inch telescope. The 5 arc minute field of the CCD does not contain enough bright catalog stars to permit direct determination of precise sky coordinates. Accordingly, eight stars from the Smithsonian Astrophysical Observatory (SAO) catalog within 1 degree of the radio position were measured on the Palomar Sky Survey, along with eight faint stars within 1 arc minute. The sky coordinates of the faint stars, calculated relative to the catalog stars, were used to establish coordinates on the CCD image. The total estimated error between radio and CCD coordinates is about 1 arc second. Two stellar objects of magnitude $(m_r) \simeq 22.5$ are offset by only 0.8 arc second from A and B, with precisely the same separation and position angle, and are undoubtedly their optical counterparts. In addition, a 23rd-magnitude diffuse object is centered near C. At this position in the sky, estimated absorption in the *r* band due to our galaxy is 0.5 magnitude, based on 21-cm neutral hydrogen column densities (*10*). If the absorption fluctuates significantly on a scale smaller than the 36-arc-minute beam of the 21-cm observations, this estimate could be far from the true value.

Spectra of A and B were obtained with the PFUEI at Palomar on 8 October 1983, along with direct exposures of 5 minutes in the *r* band and 10 minutes in the 7400 to 8400 Å *i* band (*9*). Conditions were excellent, with a seeing disk less than 1 arc second. The *r* and *i* band images are shown in Fig. 2. Given the extreme faintness of all three optical components, the fact that C is extended, and the limited time this source could be observed at that time of year, we concentrated our spectroscopic efforts on A and B. A 1.5-arc-second slit was positioned to cover A and B simultaneously, and spectra were obtained in two 3000-second exposures. The processed spectra are shown in Fig. 3. Table 2 gives the rest and observed wavelengths, redshifts, line ratios, equivalent widths, and observed widths of the five identified emission lines.

Each bin in the spectra is 10 Å wide.

The instrumental resolution, determined primarily by the projected slit width, is about 25 Å in the center and slightly worse at the ends. The root-mean-square error in fitting lines in a standard helium arc spectrum was 0.7 Å. For the strong Lyman α and C IV lines, the observed wavelength differences between A and B are only 0.7 and 0.1 Å, respectively, giving the same redshifts for A and B within 40 km/sec. The mean redshift from the Ly α and C IV lines is 3.2733 ± 0.0014, consistent with the other lines, given their greater uncertainties. Except for the Si IV–O IV blend, the lines are essentially unresolved. The excellent agreement between the two emission line spectra confirms the lensed nature of the source.

The optical continuum of B is redder than that of A, probably due to contamination of B by C. The continuum ratio S_A/S_B is 1.3 ± 0.3, determined at shorter wavelengths to minimize the effect of this contamination. The large error reflects the low continuum-to-noise ratio. The line flux ratio in Table 2 varies from line to line; however, only uncertainty in the continuum level underlying the lines has been included in the listed errors. If the spectrum of A is multiplied by 0.61 ± 0.02 and subtracted from B, no lines can be seen above the noise, demonstrating that if errors due to noise are also included, S_A/S_B = 1.64 ± 0.05 for all lines. This is clearly different than the radio ratio of 0.93 ± 0.03, based on 6- and 20-cm flux densities. The most likely explanation is differential variability between the radio and optical emission in the lensed object, coupled with different light travel times along the two ray paths. There may be other factors involved, however, and optical and radio monitoring of the object is important.

Table 1. Positions, flux densities, and spectral indices of the components of 2016+112.

Component	Radio position (1950)		S (6 cm)* (mJy)	S (20 cm) (mJy)	α(1.465, 4.885)†
	Right ascension	Declination			
A	$20^h\ 16^m\ 55\overset{s}{.}471 \pm 0.010$	$+11°\ 17'\ 46\overset{''}{.}56 \pm 0.15$	21.9	56.0	+0.78 ± 0.06
B	55.267	45.07	23.2	61.7	+0.81
C	55.329	43.35	67.9	91.2	+0.24

*Estimated flux density errors are 5 percent. 1 mJy = 10^{-29} W Hz^{-1} m^{-2}. †$\alpha = -\ln(S_6/S_{20})/\ln$ (4.885 GHz/1.465 GHz).

The morphology, color, and apparent magnitude of C from the r and i images suggest that it is a giant elliptical galaxy at a redshift of 0.80 ± 0.15 (not including the uncertainty in galactic absorption discussed previously). Consistent with this hypothesis are the strong radio emission from C, and the excess red optical continuum of B compared to A, which we interpret as contamination of B by C. It is highly likely that an elliptical galaxy at the observed location would contribute to the lensing; however, since C is not collinear with A and B, a single elliptically symmetric galaxy at C cannot by itself produce the source geometry observed. Given multiple image formation by a galaxy, noncollinearity can be produced by differential multiple bending of the ray paths by other mass concentrations close to the lines of sight (*11*), but this effect is at least an order of magnitude too small for 2016+112. Lens models similar to those for 0957+561 (*12*), consisting of a brightest cluster galaxy at C plus a substantial quantity of dark matter associated with the cluster, can reproduce the image geometry without difficulty. There is some evidence in the direct CCD images for the presence of a cluster of galaxies, but the field is crowded, and only with measured redshifts can cluster membership be determined reliably. Quantitative tests of any model must await further observations.

The surface brightness of an object is unchanged in images formed by lensing, but the solid angle of the lensed image may differ from its unlensed value, thereby changing the total observed flux in a given image. The ratio of observed flux to unlensed flux, or *magnification*, may range, in principle, from zero to infinity; however, in essentially all physical lens systems, at least one image will have a magnification greater than unity. Lensing by galaxies and clusters of galaxies must produce an odd number of images, but the magnifications may be quite different. In 2016+112, a third image of the distant object may lie near the radio core of the galaxy, contributing to the observed C component. If so, and the magnification of the third image is not too small, higher resolution observation with very long baseline interferometry may reveal C's compound nature.

The lensed nature of 2016+112 has been confirmed by the spectra of A and B, but many questions about the lensing remain. The redshift of C, and its possible parent cluster, must be determined before a reliable model can be constructed. The image magnifications can only be determined from a model. The third image must be searched for, and the possible composite nature of the source at C examined. Absorption features in

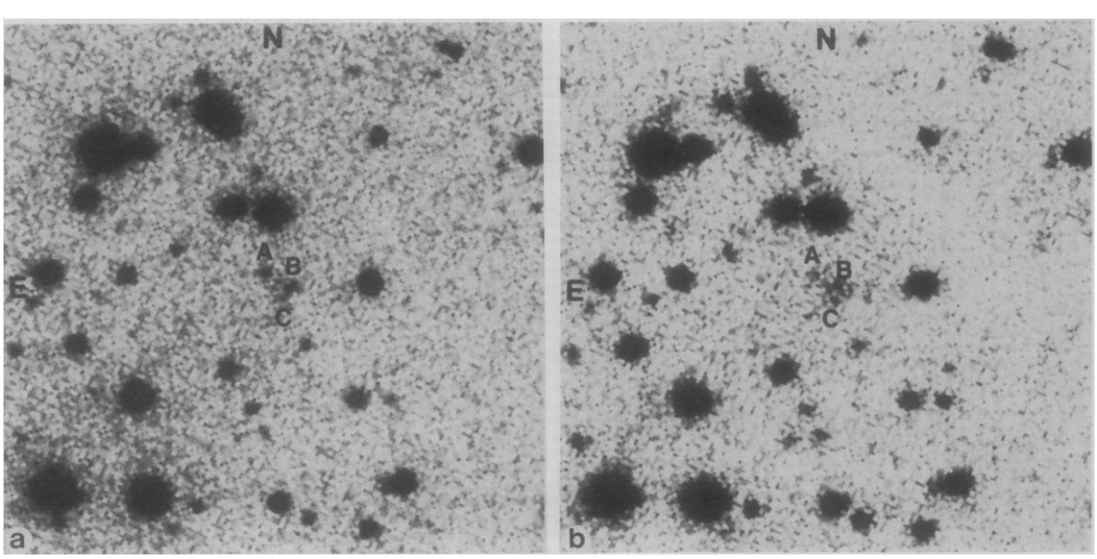

Fig. 2. Arc-minute square sections of CCD images of 2016+112, made with the 200-inch telescope on 8 October 1983: (a) r band, 5-minute integration; (b) i band, 10-minute integration.

the optical spectra, Faraday rotation of radio polarization, and the milli-arc-second radio structure all need to be determined.

The high redshift and extremely narrow emission lines of 2016+112 A and B make it an intriguing object, independent of the lensing. If assumptions are made about the shape of the continuum spectrum, radio and optical luminosities at standard rest frequencies can be calculated in terms of m, the unknown magnification, h, defined by $H_0 = 50h$ km sec^{-1} Mpc^{-1}, and q_0. Assuming that the radio spectrum is a power law with $\alpha = +0.8$, down to at least 350 MHz (observed), the radio luminosity at 1.4 GHz (rest) is 1.1×10^{27} $(m\ h^2)^{-1}$ W Hz^{-1} sr^{-1} for $q_0 = 0$, and 2.9×10^{26} $(m\ h^2)^{-1}$ W Hz^{-1} sr^{-1} for $q_0 = 1/2$. The spectral index of the optical continuum cannot be determined from our data, because of unknown but potentially large systematic color errors introduced by the uncertainty in galactic absorption and by the fact that our spectra were acquired with a slit. If the spectral index of the optical continuum is +0.5, typical of quasars (*13*), the optical luminosity at 2500 Å (rest) is 3.9×10^{23} $(m\ h^2)^{-1}$ W Hz^{-1} sr^{-1} for $q_0 = 0$, and 1.0×10^{23} $(m\ h^2)^{-1}$ W Hz^{-1} sr^{-1} for $q_0 = 1/2$. Distinctions between quasars, Seyfert galaxies, radio galaxies, and other active galactic nuclei are often blurred; even so, the lensed object does not fit neatly into any category. The radio and optical luminosities are in the quasar range, but the narrowness of the emission lines is extremely rare for quasars (*14*). The radio luminosity is at least three orders of magnitude greater than that of Seyfert galaxies (*15*), more than can be accounted for by the lens magnification. Finally, although radio galaxies often have narrow emission lines, galaxies of high radio luminosity rarely have a single radio component of small angular size. Also, radio galaxies whose optical emission is dominated by a starlike nucleus (N galaxies) are more likely to show broad emission lines than narrow ones (*16*). One of the fifteen N galaxies in the sample of Grandi and Osterbrock (*16*), however, does have both narrow lines and a single strong, compact radio component.

Even if the magnifications of A and B are only unity, a probable lower limit, the lensed object is the least luminous optical source ever observed spectroscopically at such a high redshift. Given the difficulty of the observations, however, other sources of similar nature could easily have gone undetected. It may turn out that without lens magnification, 2016+112 A,B itself would be impossible to observe optically.

As stated earlier, significant progress on the problem of the mass distribution of galaxies and clusters, and the values of the cosmological parameters, will require either a statistical sample of lenses or a few simple or special cases. We now discuss what we believe to be the best method for finding a larger sample of lenses.

Gravitational bending of radiation is

Table 2. Parameters of emission lines in the spectra of 2016+112 A and B.

Line	Component	Rest wavelength* (Å)	Observed wavelength (Å)	Redshift	Line ratio A/B†	Rest equivalent width (Å)	Width (FWHM)‡ (km/sec)
Ly α	A	1215.67	5193.8	3.2724	1.60 ± 0.04	171	< 1000
	B		5193.1	3.2718		142	
N V	A	1240.1	5303.3	3.2764	1.50 ± 0.20	39	< 1600
	B		5304.6	3.2774		36	
Si IV–O IV	A	1402	5988.0	3.2713	0.89 ± 0.49	12	
	B		5982.9	3.2677		12	
C IV	A	1549.0	6621.6	3.2746	1.44 ± 0.08	67	< 1100
	B		6621.5	3.2745		34	
He II	A	1640.5	7001.2	3.2677	0.86 ± 0.32	8.5	< 1200
	B		6994.5	3.2636		7.6	

*The N V and C IV lines are blends of two transitions separated by 4.0 and 2.5 Å, respectively. The Si IV–O IV line is a blend of many lines over a range of 10 to 15 Å. †The estimated errors reflect only uncertainty in the continuum underlying the lines. ‡The observed lines are a convolution of the true line profiles with the instrumental response profile. The instrumental profile is determined primarily by the width of the projected slit. To estimate the true line widths, Gaussians of various widths were convolved with the helium arc spectrum. The smallest Gaussian width that produced a convolved profile noticeably wider than the observed profile is given as an upper limit to the true line width.

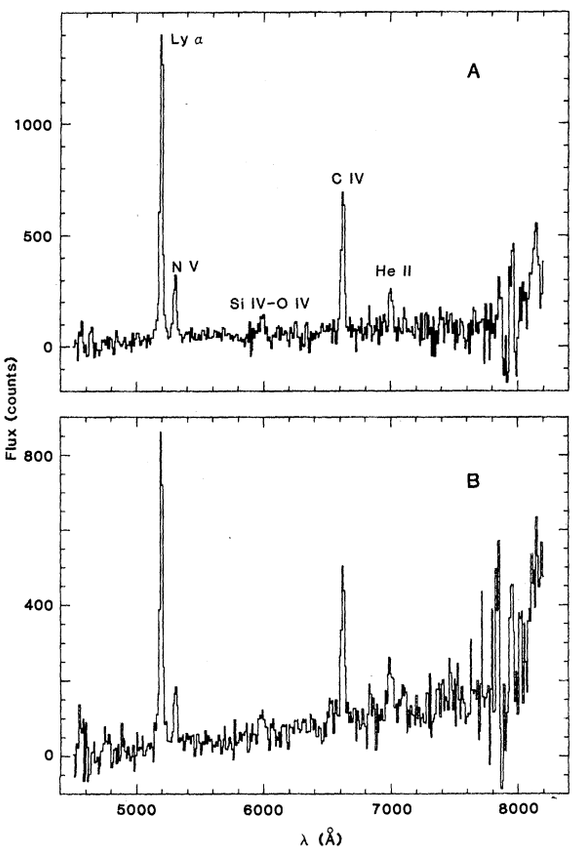

Fig. 3. Spectra of 2016+112 A and B, with 1 bin = 10 Å. The instrumental resolution is about 25 Å. On the vertical scale, 100 units = 23rd magnitude on the monochromatic AB magnitude scale (*18*), corresponding to a flux density of 2.3 μJy. The increased noise at the ends of the spectra reflects decreased sensitivity of the CCD detector at those wavelengths.

achromatic, and the signature of lensing is multiple images with identical spectra. There are three complications, however, that in practice differentially modify the spectra. First, the ray paths for the various images may have different lengths, and the images we observe simultaneously were actually emitted at different times. If the source varies, the images will not be identical. (Although a complication in identifying lenses, time delays are central in the determination of cosmological parameters from lensing.) Second, quasars and other types of active galactic nuclei may have complicated radio structure on an angular scale comparable to the angular scale of the image separations. It is possible for lensed images to show different regions of the original structure. Third, intervening matter, possibly including the lensing mass itself, may produce differential absorption along the different ray paths. The strategy for identifying lensing, then, is to look for multiple images with approximately the same spectra, and then to demonstrate that any observed differences are due to variability or details of the image formation.

It is possible to calculate the number of lens systems that should be observed in a given sample of quasars, based on the spatial distribution and masses of galaxies and the redshift distribution of the quasars in the sample. Such calculations have been made by Turner *et al.* (*17*), who conclude that between 2.3 and 5.1 out of every thousand quasars will be lensed, depending on the number density and dynamical properties of galaxies and the value of q_0. The peak in the distribution of angular separations is near 1 arc second. Since at optical wavelengths the blurring effect of the earth's atmosphere is usually of this order, optical searches for lensing are inefficient. At radio wavelengths, however, interferometers such as the VLA routinely observe with resolutions of tenths of arc seconds. In addition, although most quasars found in optical surveys are too weak as radio sources to be detected with present-day instruments, most of the constraints on models of particular lensing systems come from high-resolution radio observations. (Of the three previously reported lens systems, only 0957+561 is a detectable radio source.) Therefore, not only is a VLA search for gravitational lensing likely to be more productive than optical searches, but any lens systems found are likely to be more useful as cosmological probes than radio-weak systems.

There are four steps in a VLA search for gravitational lenses: (i) observe a source at the VLA at 6 cm. If the structure suggests lensing, (ii) observe at the VLA at a second frequency. If the two-point radio spectra of the multiple images are the same, (iii) observe the source optically. If optical images are also consistent with lensing, (iv) obtain optical spectra. 2016+112 is the first lens system found by this method, and it is evidently an extraordinary system. Its discovery did not depend on its unusual features, however, and the above procedure should provide a sample of lens systems large enough to show both the common and the anomalous characteristics of gravitational lenses.

C. R. LAWRENCE
Department of Physics, Massachusetts Institute of Technology, Cambridge 02139, and *Radio Astronomy 105-24, California Institute of Technology, Pasadena 91125*

D. P. SCHNEIDER
M. SCHMIDT
Department of Astronomy, California Institute of Technology

C. L. BENNETT
J. N. HEWITT
B. F. BURKE
Department of Physics, Massachusetts Institute of Technology

E. L. TURNER
J. E. GUNN
Princeton University Observatory, Peyton Hall, Princeton, New Jersey 08544

References and Notes

1. A. S. Eddington, *Space, Time, and Gravitation* (Cambridge Univ. Press, New York, 1920).
2. F. Zwicky, *Phys. Rev. Lett.* **51**, 290 (1937).
3. A. Einstein, *Science* **84**, 506 (1936).
4. D. Walsh, R. F. Carswell, R. J. Weymann, *Nature (London)* **279**, 381 (1979).
5. R. J. Weymann *et al.*, *ibid.* **285**, 641 (1980); D. W. Weedman, R. J. Weymann, R. F. Green, T. M. Heckman, *Astrophys. J. Lett.* **255**, L5 (1982).
6. H_0, the Hubble constant, specifies the rate of expansion of the universe; q_0, the deceleration parameter, is a dimensionless quantity that specifies how the expansion rate changes with time; and Λ, the cosmological constant, specifies the mass-energy density of the vacuum.
7. C. L. Bennett, C. R. Lawrence, B. F. Burke, in preparation.
8. NRAO is operated by Associated Universities, Inc., under contract with the National Science Foundation.
9. D. P. Schneider, J. E. Gunn, J. G. Hoessel, *Astrophys. J.* **264**, 337 (1983); T. X. Thuan and J. E. Gunn, *Publ. Astron. Soc. Pac.* **88**, 543 (1976); R. A. Wade, J. G. Hoessel, J. H. Elias, J. P. Huchra, *ibid.* **91**, 35 (1979).
10. C. Heiles, *Astron. Astrophys. Suppl.* **20**, 37 (1975).
11. J. E. Gunn, *Astrophys. J.* **147**, 61 (1967).
12. P. Young, J. E. Gunn, J. Kristian, J. B. Oke, J. A. Westphal, *ibid.* **244**, 736 (1981); P. E. Greenfield, thesis, Massachusetts Institute of Technology (1981).
13. D. O. Richstone and M. Schmidt, *Astrophys. J.* **235**, 361 (1980); B. T. Soifer, G. Neugebauer, J. B. Oke, K. Matthews, J. H. Lacy, *ibid.* **265**, 18 (1983).
14. J. Stocke, J. Liebert, T. Maccacaro, R. E. Griffiths, J. E. Steiner, *ibid.* **252**, 69 (1982).
15. A. Wilson, *Int. Astron. Union Symp. 97* (1982), pp. 179–188.
16. S. A. Grandi and D. E. Osterbrock, *Astrophys. J.* **220**, 783 (1978).
17. E. L. Turner, J. P. Ostriker, J. R. Gott, in preparation.
18. J. B. Oke, *Astrophys. J. Suppl.* **27**, 21 (1974).
19. Astronomical research at the California Institute of Technology, the Massachusetts Institute of Technology, and the Princeton University Observatory is supported by the National Science Foundation. E.L.T. is an Alfred P. Sloan Foundation Fellow.

17 November 1983; accepted 7 December 1983

Late Miocene Vegetational and Climatic Variations Inferred from a Pollen Record in Northwest Wyoming

Abstract. *A pollen stratigraphy from late Miocene lacustrine strata (Teewinot Formation) in Jackson Hole, Wyoming, permits analysis of vegetation and climate history over a time interval of less than 300,000 years with better temporal resolution of data than has been reported from terrestrial Tertiary deposits. The flora was essentially modern, and six successive pollen assemblages indicate alternating dry and wet conditions. The frequency of climatic change in this record is similar to that inferred from marine isotope records for both late Tertiary and Quaternary time.*

Major climatic fluctuations are well documented as a series of glaciations and interglaciations during the Quaternary Period, and the isotope record from marine sediments suggests that climatic cycles have occurred throughout the Cenozoic Era (*1*). Recognition of such events in nonmarine Tertiary strata has been difficult, however, since there are few long continuous records. An exception is the late Miocene Teewinot Formation (9-million-year-old lake sediments) of Jackson Hole, Wyoming. The pollen record shows that during the late Cenozoic a series of short-term vegetation changes took place as the overall aspect of climate and vegetation shifted from temperate to continental in the Rocky Mountains.

The Teewinot Formation is a sequence 2000 m thick of lacustrine sediments that outcrop in a 60-km^2 area in Jackson Hole (Fig. 1). The upper 68 m consist predominantly of interbedded calcareous claystone, siltstone, and coarse vitric tuff, which are exposed along the lower Gros Ventre River. Fossil vertebrates, mollusks, and ostracods indicate deposition in a large freshwater lake (*2*). The lake apparently occupied much of the